

Simultaneous three-dimensional optical coherence tomography and intravital microscopy for imaging subpleural pulmonary alveoli in isolated rabbit lungs

Sven Meissner

University of Technology, Dresden
Clinical Sensing and Monitoring
Faculty of Medicine Carl Gustav Carus
Fetscherstrasse 74
01307 Dresden
Germany

Lilla Knels

University of Technology, Dresden
Department of Anesthesiology and Intensive Care
Faculty of Medicine Carl Gustav Carus
Fetscherstrasse 74
01307 Dresden
Germany

Alexander Krueger

University of Technology, Dresden
Clinical Sensing and Monitoring
Faculty of Medicine Carl Gustav Carus
Fetscherstrasse 74
01307 Dresden
Germany

Thea Koch

University of Technology, Dresden
Department of Anesthesiology and Intensive Care
Faculty of Medicine Carl Gustav Carus
Fetscherstrasse 74
01307 Dresden
Germany

Edmund Koch

University of Technology, Dresden
Clinical Sensing and Monitoring
Faculty of Medicine Carl Gustav Carus
Fetscherstrasse 74
01307 Dresden
Germany

1 Introduction

1.1 Medical Background

During intensive care, mechanical ventilation of the patient often becomes necessary to avoid hypoxia and hypercapnia. Ventilator settings, which mainly control breathing rate, tidal volume, and airway pressure, are commonly chosen from standard operating procedures that take body weight and oxy-

Abstract. There is a growing interest in analyzing lung mechanics at the level of the alveoli in order to understand stress-related pathogenesis and possibly avoid ventilator associated lung injury. Emerging quantitative models to simulate fluid mechanics and the associated stresses and strains on delicate alveolar walls require realistic quantitative input on alveolar geometry and its dynamics during ventilation. Here, three-dimensional optical coherence tomography (OCT) and conventional intravital microscopy are joined in one setup to investigate the geometric changes of subpleural alveoli during stepwise pressure increase and release in an isolated and perfused rabbit lung model. We describe good qualitative agreement and quantitative correlation between the OCT data and video micrographs. Our main finding is the inflation and deflation of individual alveoli with noticeable hysteresis. Importantly, this three-dimensional geometry data can be extracted and converted into input data for numerical simulations.

© 2009 Society of Photo-Optical Instrumentation Engineers. [DOI: 10.1117/1.3247149]

Keywords: biomedical optics; alveolar mechanics; acute lung injury; lung dynamics.

Paper 09223PR received Jun. 5, 2009; revised manuscript received Jul. 22, 2009; accepted for publication Aug. 4, 2009; published online Oct. 12, 2009. This paper is a revision of a paper presented at the SPIE conference on Optical Coherence Tomography and Coherence Techniques III, June 2007, Munich, Germany. The paper presented there appears (unrefereed) in SPIE Proceedings Vol. 6627.

genation into account but do not give much consideration to lung mechanics. In a clinical study of patients suffering from adult respiratory distress syndrome,¹ the group who was ventilated with a lower tidal volume per body weight showed better survival and outcome than the conventionally ventilated group, suggesting that the normally chosen tidal volume is harmful to the preinjured lung.² The potential for ventilator-associated lung injury (VALI) and ventilator-induced lung injury (VILI) has propelled intensive research into the underlying mechanisms.^{3,4} Mechanical stress on the lung parenchyma

Address all correspondence to: Sven Meissner, Klinisches Sensing and Monitoring Medizinische Fakultät der Technischen Universität Dresden, Fetscherstraße 74, 01307 Dresden, Germany. Tel: 49-351-458-6133; Fax: 49-351-458-6325; E-mail: sven.meissner@tu-dresden.de

has been identified as a major contributor to development of VILI/VALI. This stress not only produces barotrauma and volume trauma (i.e., the rupture of alveolar walls), but also so-called biotrauma from proinflammatory signaling by the mechanically stressed alveolar epithelial and endothelium cells or from the stressed alveolar-capillary barrier. Because shear stress and stretch acting on the alveolar walls cannot be directly measured, it is essential to simply observe the geometric deformations of alveolar structures during ventilation and relate them to the ventilator settings.

1.2 Methods for Imaging Pulmonary Alveoli

Computer tomography (CT), the routine diagnostic tool for lung injury,⁵ lacks the resolution for imaging single alveoli and micro-CT need fixed and stained tissue to make measurements on an alveolar scale. Magnet resonance imaging with hyperpolarized helium only indirectly allows evaluating alveolar size.⁶ The resolution necessary to image single alveoli (diameter=50–100 μm) can presently only be reached by optical methods such as *in vivo* video microscopy (IVM) of subpleural alveoli in small animal models.^{7,8} Two-dimensional IVM images provide information in the form of bright reflections determining the projection of the outer diameter of the alveoli. These reflections can be caused by alveolar walls but also by the capillary network in the pleura or by a pleura-enforcing collagen network. Thus, interpretation of these images is not unambiguous. As a result, controversy and open questions still exist about alveolar mechanics, particularly regarding alveolar deformation during volume uptake. At least four mechanisms—all consistent with the pressure volume curve of the whole lung—have been hypothesized: (i) opening/recruitment of additional collapsed alveoli, (ii) balloonlike stretching of the alveolar wall, (iii) unfolding of the alveolar wall, and (iv) expansion of the alveolar duct connecting the alveoli.^{4,9} Direct experimental evidence of the existence of all or some of these deformation mechanisms is required before clarifying how they influence the alveolar stress level and the development of biotrauma.

To avoid the problems of IVM, particularly the image artifacts and general uncertainty about whether the optical image corresponds to actual alveolar geometry, we propose three-dimensional (3-D) alveolar imaging via optical coherence tomography (OCT). OCT provides 3-D imaging of air-filled subpleural lung tissue up to a depth of 500 μm with a resolution of <10 μm . Therefore, alveolar areas can be quantified in several accurately defined spatial planes beneath the pleura. We previously acquired cross-sectional images of subpleural alveoli in the ventilated and perfused rabbit lung and found a qualitative difference in alveolar mechanics between high tidal volume ventilation with zero end-expiratory pressure (ZEEP) and low tidal volume ventilation with high positive end-expiratory pressure (PEEP).¹⁰ Although ZEEP led to repetitive alveolar collapse and recruitment, PEEP maintained stable alveolar opening. Quantitative analysis of the alveolar cross sections, however, was hindered by shifting of the alveoli in and out of the plane during tidal ventilation that produced errors in calculating the air-filled area. Therefore, here we present 3-D OCT^{11,12} of the perfused isolated rabbit lung with stepwise increased constant positive airway pressure (CPAP). IVM images of the subpleural alveoli were also si-

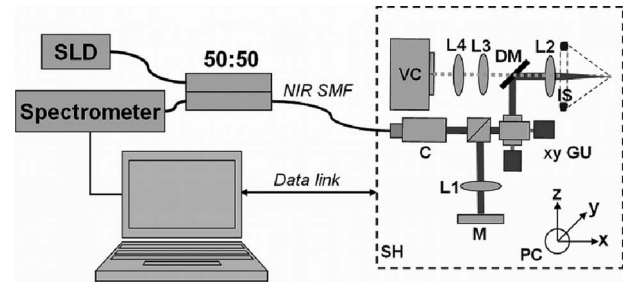


Fig. 1 Experimental setup for 3-D imaging of subpleural alveoli in isolated and perfused rabbit lungs. A fiber coupler and single-mode fibers (NIR SMF) connect the light source (SLD) centered at 840 nm (FWHM 50 nm), the interferometer integrated in the scanner head (SH) and the spectrometer. The near-infrared light (NIR) is coupled in the interferometer by a collimator and divided into reference and sample beam by a beamsplitter cube. The sample beam is deflected by a galvanometer scanner unit (GU) for the x and y direction and focused by an objective (L2) to the sample. The backscattered light is superimposed with the reference light, focused (L1) and reflected by the reference mirror (RM), and coupled in the SMF and transmitted to the spectrometer, where it is spectrally resolved by a grating (1100 lines/mm). Interference spectrum is detected by a CCD line (2048 pixels) with an acquisition rate of 12 kHz (A-scan rate). The system provides a lateral resolution of 7 μm and an axial one of 8 μm in air (6 μm in tissue, $n=0.133$). A dichroic mirror (DM) separates the light for IVM, which is then focused with lenses L3 and L4. The IVM image is acquired by a CMOS camera, which is also integrated in the SH. A ring light, consisting of 12 superhigh light-emitting diodes, is positioned at the front of the SH above the sample for illumination. The SH is mounted on a translation stage to carry out optimal positioning in front of the isolated lung. A conventional personal computer was used for data acquisition, position control, and image processing.

multaneously acquired in order to make direct qualitative and quantitative comparisons between the two methods.

2 Material and Methods

2.1 Isolated Rabbit Lungs

Use of isolated, perfused, and ventilated rabbit lung as a model has been previously described.¹⁰ All experiments were performed in accordance with Ref. 13. The lungs were initially ventilated by volume-controlled ventilation for 20 min using a KTR 4 small-animal ventilator (Hugo-Sachs, Freiburg, Germany) with a 3-cm H_2O PEEP. Respiratory rate was set at 30/min and tidal volume at 8 ml/kg body weight (bw). Spirometry was carried out using a Fleisch pneumotachograph (Hugo-Sachs, Freiburg, Germany). CPAP was applied and stepwise increased to 25 cm H_2O and then stepwise decreased to 5 cm H_2O . Pressurized air and a PEEP valve was used to adjust CPAP levels. At each CPAP level (5, 10, 15, 20, 25, 20, 15, 10, 5 cm H_2O), a 3-D-OCT ($200 \times 200 \times 512$ pixels/ $800 \times 800 \times 2048 \mu\text{m}^3$) scan was performed and an IVM micrograph (1600×1200 pixels/ $1500 \times 1150 \mu\text{m}^2$) was taken.

2.2 Combined OCT and IVM

The combined OCT-IVM system setup is shown in Fig. 1. This system is also suitable for *in vivo* investigation, as previously reported.¹⁴ Compared to our formerly used OCT system, a microscope imaging system has been added and the

system has been improved in terms of adding a galvanometer y-scanner axis, higher acquisition speed, and doubled measurement depth. The OCT light source is a fiber-coupled superluminescence diode with 1-mW output power and a 50-nm (FWHM) broad spectrum centered at 840 nm (Superlum, Moscow, Russia). The near-infrared light is guided to the scanner head with an integrated 50:50 (sample arm: reference arm) nonpolarizing beamsplitter, a reference arm adjustable in length and attenuation, two galvanometer mounted scanner mirrors (Cambridge Technology Inc., Lexington, Kentucky), a dichroic mirror separating the visible microscope light from the near-infrared light used for OCT, and a focusing objective. The backscattered near-infrared sample light is collected into the interferometer, superimposed with the reference light, and guided to the grating spectrometer. The interference spectrum is focused onto a 2048-pixel-wide charge-coupled device line camera with a 25-MHz pixel clock, 14-bit analog-to-digital conversion, and a FireWire connection to the computer (Micro-Epsilon Optronic, Langebrueck, Germany). In addition, an IVM is integrated into the system. The sample is illuminated by a ring of white light-emitting diodes. The diffuse visible reflections from the sample are imaged through the objective, the dichroic mirror, and two additional lenses onto a color complementary oxide semiconductor camera (Sumix, Oceanside, California), which is mounted to the scanner head unit and connected to the computer via a universal serial bus. The integrated OCT and IVM imaging unit and the mechanical ventilator system are all connected to the same computer. The OCT-IVM acquisition unit is mounted on a ball-and-socket mount combined with three motorized translation stages for positioning. Synchronized computer programs implemented in LabVIEW 8.2 (National Instruments, Austin, Texas) are used to acquire respiratory data (airway pressure, tidal volume, arterial pressure), microscope images, and interference spectra for OCT, and to control the translation stages and galvanometer scanners. Rescaling of the interference spectra to wave number, spectral shaping, fast Fourier transformation, and display as gray value images can either be done online for a cross-sectional preview B-mode image or offline after acquiring the spectra and saving them on hard disk. Additional image processing (despeckle, reslicing, thresholding, etc.) and quantification was performed with ImageJ (ImageJ 1.37v, National Institutes of Health, Bethesda, Maryland) and IMAQ Vision 8.2.1 (National Instruments, Austin, Texas). The IVM images were analyzed with a tablet monitor system, allowing manual tracing of alveolar boundaries with a pen. AMIRA (AMIRA 4.1.0) image analyzing software was used for 3-D reconstruction of alveolar parenchyma.

2.3 Image Processing

OCT image stacks were tilted until the plane of view was parallel to the pleura. Five slices of the stack at 40, 44, 48, 52, and 56 μm , beneath the strongest pleura reflection were taken for en face sectional analysis (Fig. 2). The image was despeckled by taking the median of the five planes along the z-axis and a 3×3 kernel median filter in the x-y plane. A histogram stretch to the full gray value dynamic range was performed. The resulting image [Fig. 2(b)] was inverted and filtered by a threshold filter based on a 32×32 kernel gray

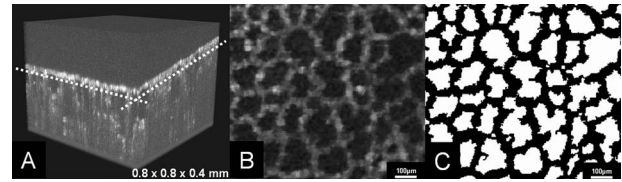


Fig. 2 Individual steps in the analysis of OCT images. (a) Volume rendered OCT image stack of subpleural alveolar lung parenchyma of an isolated rabbit lung with an applied CPAP of 25 cm H₂O. The dashed white line denotes the cutting plane of the extracted OCT en face image shown in (b). (b) Median of the five separated OCT en face images. The air-filled regions are black and the alveolar wall tissue is gray. (c) Automatic segmentation of the air-filled regions.

value histogram analysis yielding a binary image. Small areas were omitted and small holes (one pixel) were filled. The resulting image was used as a segmentation mask for separating tissue from air. Quantification of the areas of the air-filled alveolar structures was performed. The IVM images were processed with a pixel-based graphics program (Adobe Photoshop 7.0) and a graphics tablet monitor. Bright boundaries were identified as alveolar walls, manually retraced, and flood filled with the electronic pen. The resulting air-filled alveolar structures were quantified in the same way as the OCT images. IVM images and OCT sectional planes were registered by applying a fixed rescaling to the OCT images and a rigid manual registration with the IVM image. Air-filled structures present in both image types at all pressure levels were selected for quantitative comparison. Structures in contact with the image boundaries at any pressure level were not analyzed.

3 Results

3.1 Alveolar Expansion in IVM and OCT Images

To quantify alveolar expansion using images gathered via OCT, we performed a series of steps (Fig. 2). First, the volume of a 3-D OCT image series was rendered [Fig. 2(a)]. OCT en face images were then extracted from a plane beneath the *pleura visceralis* [Fig. 2(a), dashed white line], which was clearly visible as bright reflection. Here we show a representative OCT en face image from $\sim 45 \mu\text{m}$ beneath the pleura [Fig. 2(b)]. Automatic segmentation was then used to highlight the air-filled areas before quantification [Fig. 2(c)].

To compare the effectiveness of OCT versus IVM, we simultaneously obtained OCT and IVM images from identical alveolar tissue at CPAPs of 5 cm H₂O and 25 cm H₂O (Fig. 3). In the IVM images, circular and convex areas were surrounded by bright boundaries. At 5 cm H₂O CPAP, the single circular structures had diameters of $\sim 50 \mu\text{m}$ and the convex structures with several indentations were a few hundred micrometers. We thus identified these bordered areas as alveolar clusters in which the individual alveoli create the convex bulges. Qualitatively, as pressure increased the diameter of the cluster, the bulges increased and the indentations become more pronounced. Expansion caused by higher CPAP levels was noticeable using both OCT and IVM; however, the OCT technique overestimated alveolar septum thickness.

The boundaries of the alveolar clusters were used to quantify alveolar area. The increase in alveolar area as CPAP levels rose was on the same order of magnitude when detected

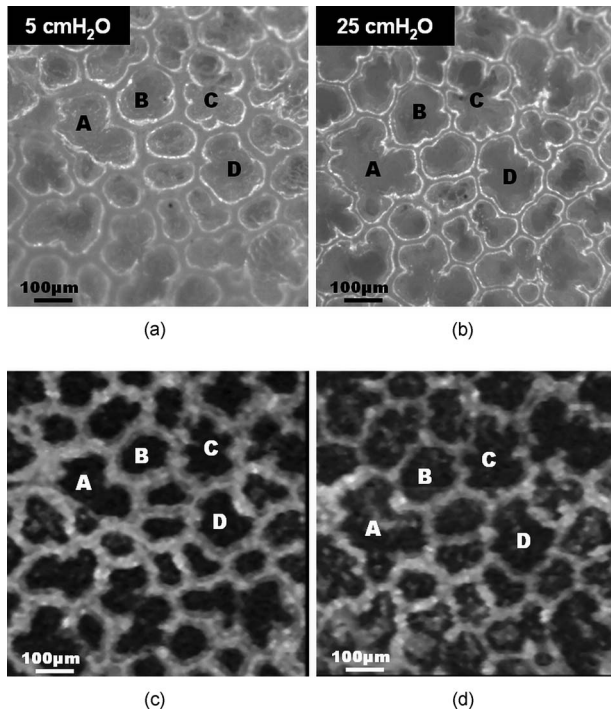


Fig. 3 Identical alveolar tissue acquired by IVM (a) and (b) or OCT (c) and (d) for an applied CPAP of 5 (a) and (c) and 25 cm H₂O (b) and (d). OCT en face images (d) representing alveolar structures of 45 µm beneath the *pleura visceralis*. Identical alveolar clusters designated as (a) to (d).

by either OCT or IVM. Alveolar expansion was found to be about 40% for IVM and 50% for OCT. When changes in alveolar area during inflation and deflation were quantified and plotted, both OCT and IVM images also revealed hysteresis behavior (Fig. 4). Plots of the alveolar area versus CPAP level for OCT and IVM were normalized to the area measured at 5 cm H₂O CPAP in the inspiratory phase. A typical *p-v* curve shape was obtained, where inflation has a constant slope between two inflection points and deflation stays on a moderately tilted plateau until it drops steeply, except at the 10-cm H₂O pressure level. In all cases, different slopes were found for pressure increase and decrease. We found curve progres-

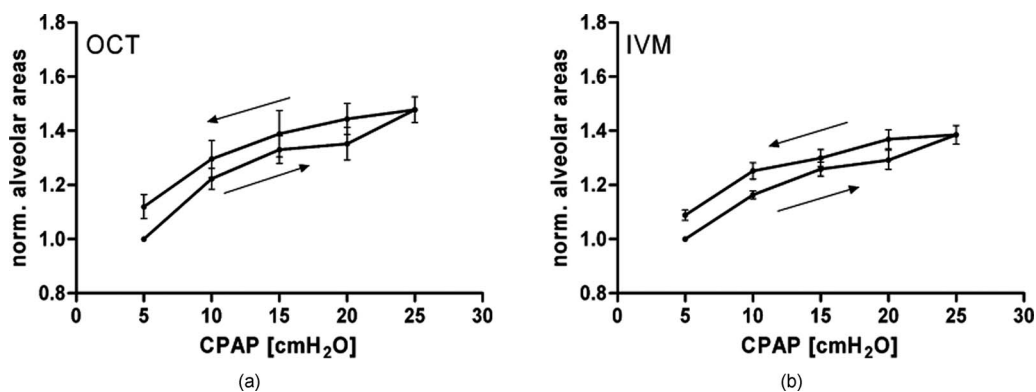


Fig. 4 Alveolar area change for increasing and decreasing CPAP measured by (a) OCT and (b) IVM. All areas are normalized to the area measured at an applied CPAP of 5 cm H₂O in the inspiratory phase. Both methods show similar results, alveolar areas enlarge with increasing CPAP and contract by decreasing CPAP. The alveolar area change is non-linear and obeys hysteresis. (*n*=4 lungs)

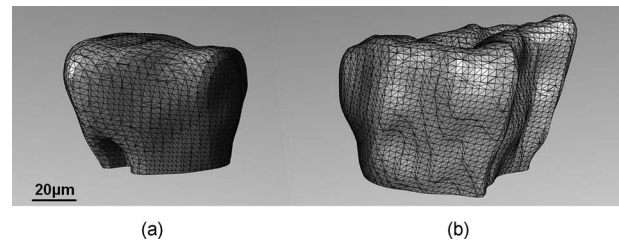


Fig. 5 Volume uptake of a single alveolar structure applying CPAP of (a) 5 cm H₂O (left) and (b) 25 cm H₂O. The volume increase is evident for higher CPAP levels. 3-D OCT data sets enable calculation of 3-D triangular meshes of the alveolar geometry, as shown here.

sion to correlate between OCT and IVM. Both curves showed hysteresis behavior during increasing and decreasing CPAP levels, indicating that the parenchyma has nonlinear (nonelastic) behavior that has a possible memory effect in the tissue. We recognized that the deflation curve does not return to baseline area CPAP of 5 cm H₂O. We also observed no recruitment or derecruitment activities in healthy lungs because the number of alveoli in the investigation area was constant at all CPAP levels.

Because OCT is a 3-D imaging technique, as opposed to 2-D IVM imaging, the acquired data sets enable 3-D reconstruction of subpleural alveolar structures. Figure 5 shows a 3-D reconstruction of an individual alveolus at an applied CPAP of 5 and 25 cm H₂O. This technique reveals the alveolar expansion in all spatial directions. Additionally, we calculated 3-D triangular meshes to describe the alveolar structures (Fig. 5, overlay). Production of these meshes is an essential precondition to developing numerical models for simulating ventilation at the level of the alveoli.

3.2 Comparison of Both OCT and IVM

To directly compare OCT and IVM techniques, we used a Bland Altman plot (Fig. 6).¹⁵ We performed linear regression and obtained a regression line with a slope of ~0.17 (Fig. 6, black line). Thus, absolute alveolar area as measured via OCT is 17% (*p*<0.001) smaller than IVM.

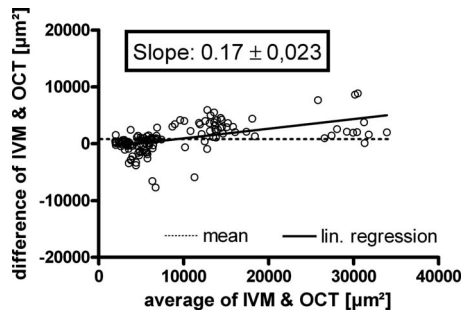


Fig. 6 Comparison of both imaging techniques using a Bland-Altman plot. The regression line is black and has a slope of 0.17. Measurements taken from OCT are $\sim 17\%$ smaller than from IVM. The detected bias is $615.5 \mu\text{m}^2$.

4 Discussion

Here, we successfully combine OCT and IVM in one setup. This offers a number of advantages for analyzing alveolar mechanics, particularly a cross-sectional view at a freely selectable depth beneath the pleura and confirmation that circular structures observed via IVM are real alveoli. On the other hand, the isolated lung model does not reflect an *in vivo* situation because both pulmonary and thoracic components constituted the respiratory pressure volume curve. Furthermore, the fact that the deflation curve does not return to baseline area of 5 cm H₂O could imply a progressive alveolar volume uptake when applying CPAP for longer times. We used our setup to observe alveolar expansion in a cross-sectional area in response to rising pressure and revealed the nonelastic mechanics of this process. Our results agree with the alveolar expansion observed in a previous studies using confocal laser scanning microscopy to image alveolar tissue in isolated lungs^{16,17} and microscopic imaging of strained lung tissue blocs.¹⁸ The detected hysteresis between inflation and deflation matches well with the physiological quasi-respiratory pressure volume curves *in vivo*.¹⁹ However, there are differences compared to *in vivo* IVM analysis of healthy and injured lungs,²⁰ suggesting alveoli do not change in volume. One important factor in our study is the deficiency of coverslips to avoid artifacts, such as deformation of alveolar geometry by suction or pressure. Our combined setup also ensures that movements in or out the focal plane cannot be misinterpreted as the recruitment of previously collapsed alveoli.

The isolated lung model and constant airway pressure procedure do have advantages over *in vivo* experiments, such as easy synchronization with imaging, lack of focusing problems, and control over physiological parameters without systemic effects. However, findings on alveolar mechanics in the stepwise inflated isolated lung cannot be generalized to *in vivo* dynamics. In principle, IVM and OCT methods, alone or in combination, are applicable *in vivo* using a transparent thorax window if the image synchronization and focusing problems can be solved. The best correlation between both techniques was observed using OCT en face images from $\sim 45 \mu\text{m}$ beneath the pleura because the alveolar area measured at this depth is approximately the equatorial area of the alveoli, assuming the alveolar diameter is $100 \mu\text{m}$.

The difference between OCT- and IVM-derived measurements of air-filled areas might be due to several reasons. One

reason might be the different transversal resolution that results in OCT overestimating alveolar wall thickness and, as a consequence, underestimating the air-filled regions. IVM images show the maximum expansion of the alveoli in the *xy* plane. This contrasts to OCT en face images, which represent the actual spatial plane and always result in smaller alveolar areas. The automatic segmentation generated for images also results in quantification differences of the alveolar clusters. The larger relative expansion measured by OCT is probably caused by overestimating alveolar wall thickness. This also underrates the air-filled areas of smaller alveolar clusters in comparison to larger clusters. In this case, the systematic mistake in measuring air-filled areas is more pronounced for alveoli during an applied CPAP of 5 cm H₂O than 25 cm H₂O. Our normalization of the air-filled area size to that at 5 cm H₂O leads to an apparently larger expansion measured in OCT images.

Here, we demonstrate that it is possible to carry out spatial segmentation of single alveolar clusters based on 3-D OCT data sets and use this data to 3-D reconstruct subpleural alveolar structures. It should be noted that speckle artifacts typical for OCT imaging hinder the exact segmentation of the air-filled spaces in the OCT data sets. OCT systems with higher resolution and faster acquisition times should improve OCT image quality and thus improve segmentation quality. Importantly, as we illustrate here, the simultaneous IVM and OCT setup has the potential to provide dynamic geometry data of alveolar structures as basis for numerical models of the lung at the level of the alveoli.

Acknowledgments

This project was supported by the German Research Foundation (DFG) "Protective Artificial Respiration" No. KO 1814/6-1.

References

1. K. F. Udobi, E. Childs, and K. Touijer, "Acute respiratory distress syndrome," *Am. Fam. Physician* **67**, 315–322 (2003).
2. Acute Respiratory Distress Syndrome Network, "Ventilation with lower tidal volumes as compared with traditional tidal volumes for acute lung injury and the acute respiratory distress syndrome," *N. Engl. J. Med.* **342**, 1301–1308 (2000).
3. J. A. Frank and M. A. Matthay, "Science review: mechanisms of ventilator-induced injury," *Crit. Care* **7**, 233–241 (2003).
4. D. Carney, J. DiRocco, and G. Nieman, "Dynamic alveolar mechanics and ventilator-induced lung injury," *Crit. Care Med.* **33**, S122–S128 (2005).
5. L. M. Malbouisson, J. C. Muller, J. M. Constantin, Q. Lu, L. Puybasset, and J. J. Rouby, "Computed tomography assessment of positive end-expiratory pressure-induced alveolar recruitment in patients with acute respiratory distress syndrome," *Am. J. Respir. Crit. Care Med.* **163**, 1444–1450 (2001).
6. E. van Beek, J. M. Wild, H. U. Kauczor, W. Schreiber, J. P. Mugler, and E. E. de Lange, "Functional MRI of the lung using hyperpolarized 3-helium gas," *J. Magn. Reson. Imaging* **20**, 540–554 (2004).
7. B. D. Daly, G. E. Parks, C. H. Edmonds, C. W. Hibbs, and J. C. Norman, "Dynamic alveolar mechanics as studied by videomicroscopy," *Respir. Physiol.* **24**, 217–232 (1975).
8. H. J. Schiller, U. G. McCann, D. E. Carney, L. A. Gatto, J. M. Steinberg, and G. F. Nieman, "Altered alveolar mechanics in the acutely injured lung," *Crit. Care Med.* **29**, 1049–1055 (2001).
9. R. D. Hubmayr, "Perspective on lung injury and recruitment: a skeptical look at the opening and collapse story," *Am. J. Respir. Crit. Care Med.* **165**, 1647–1653 (2002).
10. A. Popp, M. Wendel, L. Knels, T. Koch, and E. Koch, "Imaging of the three-dimensional alveolar structure and the alveolar mechanics

- of a ventilated and perfused isolated rabbit lung with Fourier transform optical coherence tomography," *J. Biomed. Opt.* **11**(1), 14015 (2006).
11. A. F. Fercher, W. Drexler, C. K. Hitzenberger, and T. Lasser, "Optical coherence tomography—principles and applications," *Rep. Prog. Phys.* **66**, 239–303 (2003).
 12. D. Huang, E. A. Swanson, C. P. Lin, J. S. Schuman, W. G. Stinson, W. Chang, M. R. Hee, T. Flotte, K. Gregory, C. A. Puliafito, and J. G. Fujimoto, "Optical coherence tomography," *Science* **254**, 1178–1181 (1991).
 13. *Guide for the Care and Use of Laboratory Animals*, 7th ed., Institute of Laboratory Animal Resources, National Academy Press, Washington, DC (1996).
 14. S. Meissner, M. Mertens, A. Krüger, A. Tabuchi, W. Kuebler, and E. Koch, "In vivo three-dimensional Fourier domain optical coherence tomography of subpleural alveoli combined with intra vital microscopy in the mouse model," in *Biomedical Optics*, OSA Technical Digest (CD), Optical Society of America, Paper No. BWF4, (2008).
 15. J. M. Bland and D. G. Altman, "Measuring agreement in method comparison studies," *Stat. Methods Med. Res.* **8**, 135–160 (1999).
 16. C. E. Perlman and J. Bhattacharya, "Alveolar expansion imaged by optical sectioning microscopy," *J. Appl. Physiol.* **103**, 1037–1044 (2007).
 17. E. Namati, J. Thiesse, J. de Ryk, and G. McLennan, "Alveolar dynamics during respiration: are the pores of Kohn a pathway to recruitment?," *Am. J. Respir. Cell Mol. Biol.* **38**(5), 572–578 (2008).
 18. K. K. Brewer, H. Sakai, A. M. Alencar, A. Majumdar, S. P. Arold, K. R. Lutchen, E. P. Ingenito, and B. Suki, "Lung and alveolar wall elastic and hysteretic behavior in rats: effects of *in vivo* elastase treatment," *J. Appl. Physiol.* **95**, 1926–1936 (2003).
 19. B. Jonson and C. Svantesson, "Elastic pressure-volume curves: what information do they convey?," *Thorax* **54**, 82–87 (1999).
 20. J. D. DiRocco, D. E. Carney, and G. F. Nieman, "Correlation between alveolar recruitment/derecruitment and inflection points on the pressure-volume curve," *Intensive Care Med.* **33**, 1204–1211 (2007).